



Department of Physics & Astronomy
Experimental Particle Physics Group
Kelvin Building, University of Glasgow,
Glasgow, G12 8QQ, Scotland
Telephone: +44 (0)141 339 8855 Fax: +44 (0)141 330 5881

GLAS-PPE/98-02
May 1998

QCD at HERA

N. H. Brook

on behalf of the ZEUS & H1 collaborations

Abstract

A review of HERA measurements of structure functions, fragmentation functions and forward jet production is presented.

*invited talk given at the
2nd Latin American Symposium
on High Energy Physics,
San Juan, Puerto Rico.
Apr 8-11, 1998*

1 DIS kinematics

The event kinematics of deep inelastic scattering, DIS, are determined by the negative square of the four-momentum transfer at the lepton vertex, $Q^2 \equiv -q^2$, and the Bjorken scaling variable, $x = Q^2/2P \cdot q$, where P is the four-momentum of the proton. In the quark parton model (QPM), the interacting quark from the proton carries the four-momentum xP . The variable y , the fractional energy transfer to the proton in its rest frame, is related to x and Q^2 by $y \simeq Q^2/xs$, where \sqrt{s} is the positron-proton centre of mass energy. Because the H1 and ZEUS detectors are almost hermetic the kinematic variables x and Q^2 can be reconstructed in a variety of ways using combinations of positron and hadronic system energies and angles [1].

Neutral current (NC) DIS occurs when an uncharged boson (γ, Z^0) is exchanged between the lepton and proton. In QPM there is a 1+1 parton configuration, fig. 1a, which consists of a single struck quark and the proton remnant, denoted by “+1”. At HERA energies there are significant higher-order quantum chromodynamic (QCD) corrections: to leading order in the strong coupling constant, α_s , these are QCD-Compton scattering (QCDC), where a gluon is radiated by the scattered quark and boson-gluon-fusion (BGF), where the virtual boson and a gluon fuse to form a quark-antiquark pair. Both processes have 2+1 partons in the final state, as shown in fig. 1. There also exists calculations for the higher, next-to-leading (NLO) processes.

HERA provides a unique opportunity to study the scale behaviour of Quantum Chromodynamics in a single experiment with a cleaner background environment than that obtainable at hadron colliders. The data presented here were taken in 1994 and onwards at the ep collider HERA using the H1 and ZEUS detectors. During this period HERA operated with positrons of energy $E_e = 27.5$ GeV and protons with energy 820 GeV. A detailed descriptions of the H1 and ZEUS detectors can be found in refs. [2] and [3] respectively.

2 Structure functions

Perturbative QCD (pQCD) does not predict the absolute value of the parton densities within the proton but determines how they vary from a given input. For a given initial distribution at a particular scale, Q_0^2 , Altarelli-Parisi (DGLAP) evolution [4] enables the distributions at higher Q^2 to be determined. DGLAP evolution resums the leading $\log(Q^2)$ contributions associated with a chain of gluon emissions. At large enough positron-proton centre-of-mass energies there is a second large variable $1/x$ and, therefore, it is also necessary to resum the $\log(1/x)$ contributions. This is achieved by using the BFKL equation [5]. In the DGLAP parton evolution scheme the parton cascade follows a strong ordering in transverse momentum $p_{Tn}^2 \gg p_{Tn-1}^2 \gg \dots \gg p_{T1}^2$, while there is only a soft (kinematical) ordering for the fractional momentum $x_n < x_{n-1} < \dots < x_1$ (see figure 2.) By contrast, in the BFKL scheme the cascade follows a strong ordering in fractional momentum $x_n \ll x_{n-1} \ll \dots \ll x_1$, while there is no ordering in transverse momentum.

At small x the dominant parton is the gluon and the description of the structure function is driven by the behaviour of the gluon. Because of gluon splitting, $g \rightarrow q\bar{q}$, pQCD suggests the small x behaviour of the sea quark and gluon distributions are strongly correlated.

The kinematic plane covered by HERA and the fixed target measurements is shown in fig. 3. HERA has increased the reach in Q^2 by about 2 orders of magnitude and can also probe nearly 3 orders of magnitude further down in x . The low x region is correlated with low values of Q^2 . The differential NC DIS cross section is related to three structure functions:

$$\frac{d^2\sigma^{e^\pm p}}{dx dQ^2} = \frac{2\pi\alpha^2}{xQ^4} (Y_+ F_2(x, Q^2) - y^2 F_L(x, Q^2) \mp Y_- x F_3(x, Q^2)), \quad (1)$$

where $Y_\pm = 1 \pm (1 - y)^2$. The structure function F_2 in QPM is just the sum of the quark densities multiplied by the appropriate electric charge; F_3 arises from the weak part of the cross section and is negligible for $Q^2 < 5000$ GeV², and F_L is the longitudinal structure function and only becomes important for $y > 0.6$. Hence by measuring the differential cross section at HERA one is effectively measuring the structure function F_2 .

The F_2 measurements are shown in figs. 4 and 5 as a function of x and Q^2 respectively. The error bars are at the 5-10% level and the normalisation uncertainty is $\sim 2\%$. There is a steep rise of F_2 with decreasing x in all Q^2 bins, fig. 4. Scaling violations in Q^2 are clearly seen in fig. 5. Both H1 and ZEUS have performed next to leading order (NLO) QCD fits [6, 7] based on the DGLAP evolution equations using both HERA and fixed target data. Fig. 5 shows that these QCD fits describe the F_2 data well, though it should be noted that the data can also be satisfactorily described by the BFKL prediction [8].

The scaling violations from the HERA data allow an estimate of the gluon density $xg(x)$ at low values of x , whilst the fixed target data are used to constrain the high x region. The extracted gluon densities from the fits are shown in fig 6 for a fixed $Q^2 = 20$ GeV². The error band shows the statistical and systematic uncertainty taking into account correlations and variations in the mass of the charm quark, m_c , and the strong coupling

constant, α_s . The results of the two HERA experiments are in good agreement and the extracted densities agree with the results of NMC [9] for large x . The resulting gluon distributions show a clear rise with decreasing x and have a 15% uncertainty at $x \sim 5 \times 10^{-4}$. These NLO QCD fits are also in good agreement with the global QCD analyses performed by MRS [10] and CTEQ [11], whilst the prediction from the dynamical evolution of GRV [12] is too steep for $x < 10^{-3}$.

3 Forward Jet Production in DIS

The F_2 measurements fail to distinguish between DGLAP and the BFKL approach to the QCD evolution. The hadronic final states are expected to give additional information. For events at low x , hadron production between the current jet and the proton remnant is expected to be sensitive to the effects of BFKL or DGLAP dynamics. A possible signature of BFKL dynamics is the behaviour of DIS events at low x which contain a jet that has a transverse momentum $p_T^2(j) \approx Q^2$ (so minimizing the phase space available for DGLAP evolution) and has longitudinal momentum fraction (of the proton) x_{jet} that is large (in order to maximise the phase space for BFKL evolution), fig 2.

In Fig. 7, recent data from H1 [13] and ZEUS [14] are compared with BFKL predictions [16] and fixed order QCD predictions as calculated with the MEPJET [15] program at NLO. The conditions $p_T(j) \simeq Q$ and $x_{jet} \gg x$ are satisfied in the two experiments by slightly different selection cuts. H1 selects events with a forward jet of $p_T(j) > 3.5$ GeV (in the angular region $7^\circ < \theta(j) < 20^\circ$) with

$$0.5 < p_T(j)^2/Q^2 < 2, \quad x_{jet} \simeq E_{jet}/E_{proton} > 0.035; \quad (2)$$

while ZEUS triggers on somewhat harder jets of $E_T(j) > 5$ GeV and $\eta(j) < 2.6$ with

$$0.5 < p_T(j)^2/Q^2 < 2, \quad x_{jet} = p_z(j)/E_{proton} > 0.036. \quad (3)$$

Fig. 7 shows that both experiments observe a forward jet cross section which rises steeply with decreasing x with substantially more forward jet events than expected from NLO QCD (labelled as Born in fig. 7a.) A BFKL calculation (the stars) gives a better agreement with the data. The overall normalisation in this calculation is uncertain and the agreement may be fortuitous. Indeed, it should also be noted that both experiments observe more centrally produced dijet events than predicted by the NLO QCD calculations. The ARIADNE Monte Carlo (CDM) model describes the steeply increasing jet cross section with decreasing x . The ARIADNE model does not have a strong ordering in transverse momentum in the QCD cascade, akin to BFKL type dynamics, although it does not make explicit use of the BFKL equation. Whilst those models that adhere to the DGLAP formalism (LEPTO and HERWIG) fail to predict this large growth. Further careful investigation is necessary before claiming that BFKL is the mechanism for this enhanced forward jet production.

4 Fragmentation Functions

Fragmentation functions represent the probability for a parton to fragment into a particular hadron carrying a certain fraction of the parton's energy and, like structure functions, cannot be calculated in perturbative QCD, but can be evolved from a starting distribution at a defined energy scale. If the fragmentation functions are combined with the cross sections for the inclusive production of each parton type in the given physical process, predictions can be made for the scaled momentum, x_p , spectra of final state hadrons. Small x_p fragmentation is significantly affected by the coherence (destructive interference) of soft gluons [17], whilst scaling violation of the fragmentation function at large x_p allows a measurement of α_s [18].

A natural frame in which to study the dynamics of the hadronic final state in DIS is the Breit frame [19]. In this frame the exchanged virtual boson is purely space-like with 3-momentum $\mathbf{q} = (0, 0, -Q)$, the incident quark carries momentum $Q/2$ in the positive Z direction, and the outgoing struck quark carries $Q/2$ in the negative Z direction. A final state particle has a 4-momentum p^B in this frame, and is assigned to the current region if p_Z^B is negative, and to the target frame if p_Z^B is positive. The advantage of this frame lies in the maximal separation of the outgoing parton from radiation associated with the incoming parton and the proton remnant, thus providing the optimal environment for the study of the fragmentation of the outgoing parton.

In e^+e^- annihilation the two quarks are produced with equal and opposite momenta, $\pm\sqrt{s}/2$. This can be compared with a quark struck from within the proton with outgoing momentum $-Q/2$ in the Breit frame. In the direction of the struck quark (the current fragmentation region) the particle momentum spectra, $x_p = 2p^B/Q$, are expected to have a dependence on Q similar to those observed in e^+e^- annihilation [20, 21, 22] at energy $\sqrt{s} = Q$.

In fig 8 the $\log(1/x_p)$ distributions for charged particles in the current fragmentation region of the Breit frame are shown as a function of Q^2 . These distributions are approximately Gaussian in shape with mean charged multiplicity given by the integral of the distributions. As Q^2 increases the multiplicity increases and the the peak of the distributions shifts to larger values of $\log(1/x_p)$. Figure 9 shows this peak position, $\log(1/x_p)_{max}$, as a function of Q for the HERA data and of \sqrt{s} for the e^+e^- data. Over the range shown the peak moves from $\simeq 1.5$ to 3.3. The HERA data points are consistent with those from TASSO and TOPAZ and a clear agreement in the rate of growth of the HERA points with the e^+e^- data at higher Q is observed.

The increase of $\log(1/x_p)_{max}$ can be approximated phenomenologically by the straight line fit $\log(1/x_p)_{max} = b \log(Q) + c$ also shown in figure 9. The values obtained from the fit to the ZEUS data are $b = 0.69 \pm 0.01(\text{stat}) \pm 0.03(\text{sys})$ and $c = 0.56 \pm 0.02^{+0.08}_{-0.09}$. The gradient extracted from the OPAL and TASSO data is $b = 0.653 \pm 0.012$ (with $c = 0.653 \pm 0.047$) which is consistent with the ZEUS result. This value is consistent with that published by OPAL, $b = 0.637 \pm 0.016$, where the peak position was extracted using an alternative method [23]. A consistent value of the gradient is therefore determined in DIS and e^+e^- annihilation experiments.

Also shown is the statistical fit to the data when $b = 1$ ($c = 0.054 \pm 0.012$) which would be the case if the QCD cascade was of an incoherent nature, dominated by cylindrical phase space. The observed gradient is clearly inconsistent with $b = 1$ and therefore inconsistent with cylindrical phase space.

The inclusive charged particle distribution, $1/\sigma_{tot} d\sigma/dx_p$, in the current fragmentation region of the Breit frame are shown in bins of x_p and Q^2 in fig. 10. The increasingly steep fall-off, at fixed Q^2 , towards higher values of x_p as Q^2 increases, shown in figure 10, corresponds to the production of more particles with a smaller fractional momentum, and is indicative of scaling violation in the fragmentation function. For $Q^2 > 80 \text{ GeV}^2$ the distributions rise with Q^2 at low x_p and fall-off at high x_p and high Q^2 . In figure 10 the HERA data are compared at $Q^2 = s$ to e^+e^- data [25], again divided by two to account for the production of both a q and \bar{q} . In the Q^2 range shown there is good agreement between the current region of the Breit frame in DIS and the e^+e^- experiments.

5 Summary

This review gives a brief summary of a small sample of the QCD results coming from HERA. Charged particle distributions have been studied in the current region of the Breit frame over a wide range of Q^2 . These result show clear evidence for scaling violation in scaled momenta as a function of Q^2 and supports the coherent nature of QCD cascades. The observed charged particle spectra are consistent with the universality of quark fragmentation in e^+e^- and DIS.

The intriguing rise of F_2 at small x can be well described using conventional DGLAP evolution equations. The data though can also be described by the BFKL approach thus giving rise to ambiguities how to treat QCD in this small x regime. In order to resolve these ambiguities jet production in the forward direction has been studied and the cross section for such jets is seen not to be reproduced by Monte Carlo models based on DGLAP parton shower evolution.

References

- [1] S. Bentvelsen, J. Engelen and P. Kooijman, Proceedings of the 1991 Workshop on Physics at HERA, DESY Vol. 1 (1992) 23.
- [2] H1 Collaboration, I. Abt et al., DESY preprint 93-103, *Nucl. Instr. Meth.* **386**, 310 (1997) (Vol 1) and *ibid.* p.348 (Vol 2).
- [3] ZEUS Collab., The ZEUS Detector, Status Report 1993, DESY 1993.
- [4] G. Altarelli and G. Parisi, *Nucl. Phys.* **126**, 297 (1977); V.N. Gribov and L.N. Lipatov, *Sov. J. Nucl. Phys.* **15**, 438 and 675 (1972); Yu. L. Dokshitzer, *Sov. Phys. JETP***46**, 641 (1977).
- [5] E.A. Kuraev, L.N. Lipatov and V.S. Fadin, *Sov. Phys. JETP* **45**, 199 (1977); Y.Y. Balitsky and L.N. Lipatov, *Sov. J. Nucl. Phys.* **28**, 282 (1978).
- [6] H1 collab., Paper 262 presented at Int. Europhysics Conf. on High Energy Physics, HEP97, Jerusalem.
- [7] M. A. J. Botje, Proc. of 5th Int. workshop on DIS and QCD (1997), (eds. Repond and Krakauer).
- [8] A. J. Askew *et al.* *Phys. Rev.* **D47**, 3775 (1993); **D49**, 4402 (1994).
- [9] NMC collab., M. Arneodo *et al.* *Phys. Lett.* **B309**, 222 (1993).

- [10] A. Martin, R. Roberts and W. J. Stirling, *Phys. Lett.* **B387**, 419 (1996).
- [11] H. L. Lai *et al.*, *Phys. Rev.* **D55**, 1280 (1997).
- [12] M. Glück, E. Reya and A. Vogt, *Z. Phys.* **C67**, 433 (1995).
- [13] H1 collab., paper pa03-049 submitted to 28th Int. Conf. on High Energy Physics ICHEP'96, Warsaw, Poland.
- [14] ZEUS collab., J. Breitweg *et al.* DESY preprint 98-050.
- [15] E. Mirkes and D. Zeppenfeld, *Phys. Lett.* **B380**, 205 (1996).
- [16] J. Bartels *et al.* *Phys. Lett.* **B384**, 300 (1996).
- [17] Yu. Dokshitzer, V. Khoze, A. Mueller and S. Troyan, "Basics of Perturbative QCD", Editions Frontières, Gif-sur-Yvette, France (1991).
- [18] G. Altarelli *et al.*, *Nucl. Phys.* **B160**, 301 (1979); P. Nason and B. R. Webber, *Nucl. Phys.* **B421**, 473 (1994).
- [19] R.P. Feynman, "Photon-Hadron Interactions", Benjamin, N.Y. (1972).
- [20] Yu. Dokshitzer *et al.*, *Rev. Mod. Phys.* **60**, 373 (1988).
- [21] A. V. Anisovich *et al.*, *Il Nuovo Cimento* **A106**, 547 (1993).
- [22] K. Charchuła, *J. Phys.* **G19**, 1587 (1993).
- [23] OPAL Collab., M. Akrawy *et al.*, *Phys. Lett.* **B247**, 617 (1990).
- [24] TOPAZ collab., R. Itoh *et al.*, *Phys. Lett.* **B345**, 335 (1995).
- [25] TASSO Collab., W. Braunschweig *et al.*, *Z. Phys.* **C47**, 187 (1990); MARK II Collab., A. Petersen *et al.*, *Phys. Rev.* **D37**, 1 (1988); AMY Collab., Y. K. Li *et al.*, *Phys. Rev.* **D41**, 2675 (1990); DELPHI Collab., P. Abreu *et al.*, *Phys. Lett.* **B311**, 408 (1993).

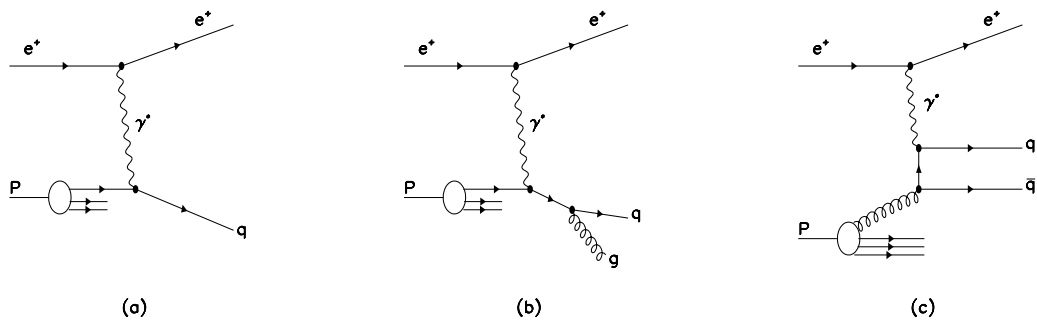


Figure 1: (a) QPM (b) QCDC and (c) BGF diagrams

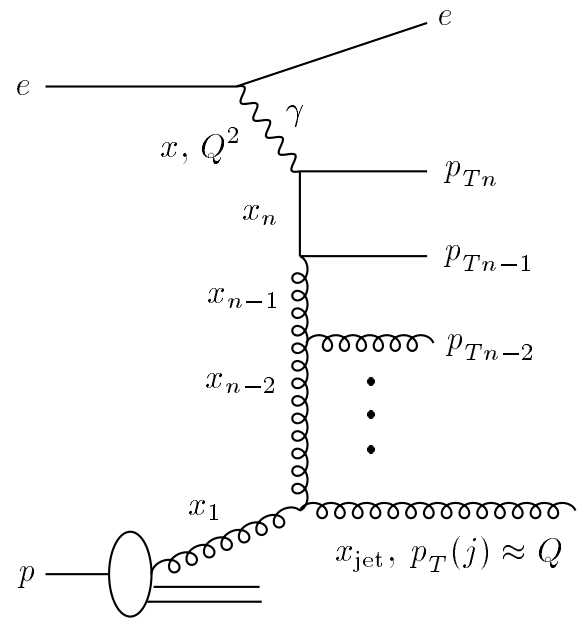


Figure 2: Parton ladder diagram in DIS.

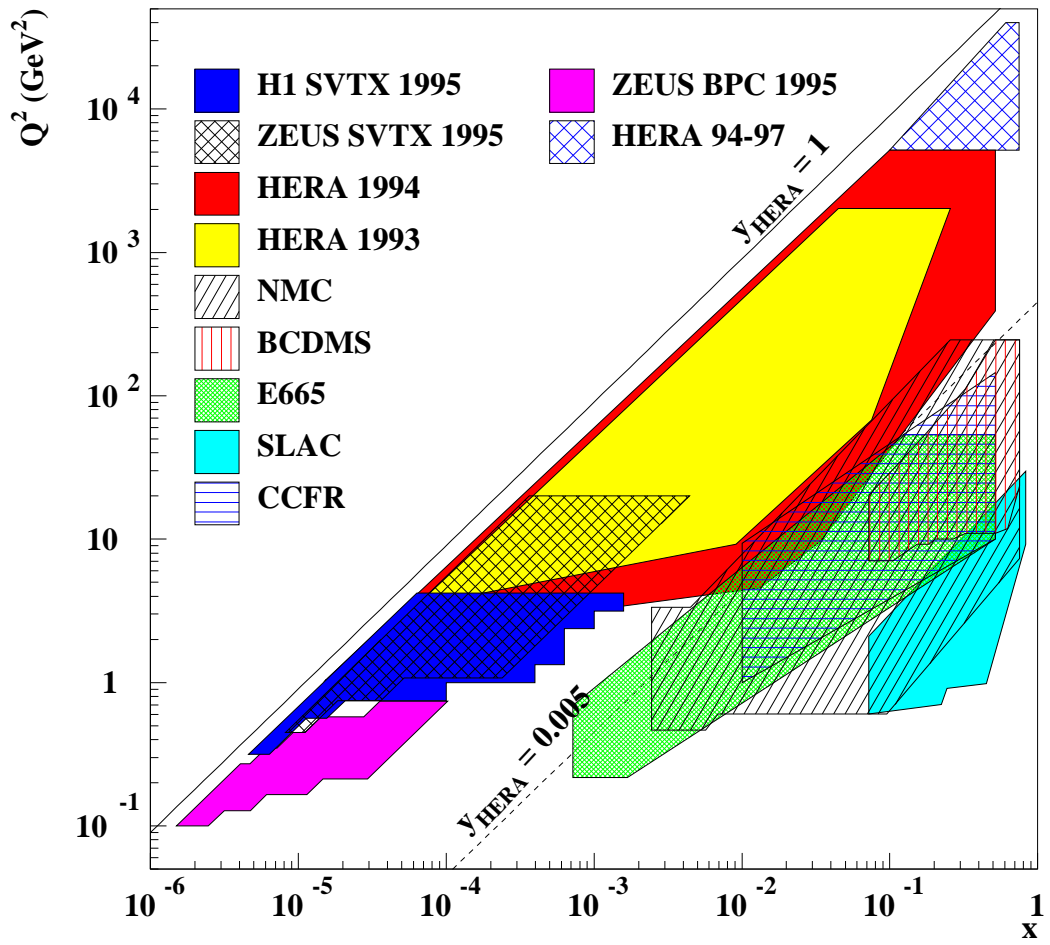


Figure 3: The kinematical region covered by HERA and fixed target experiments

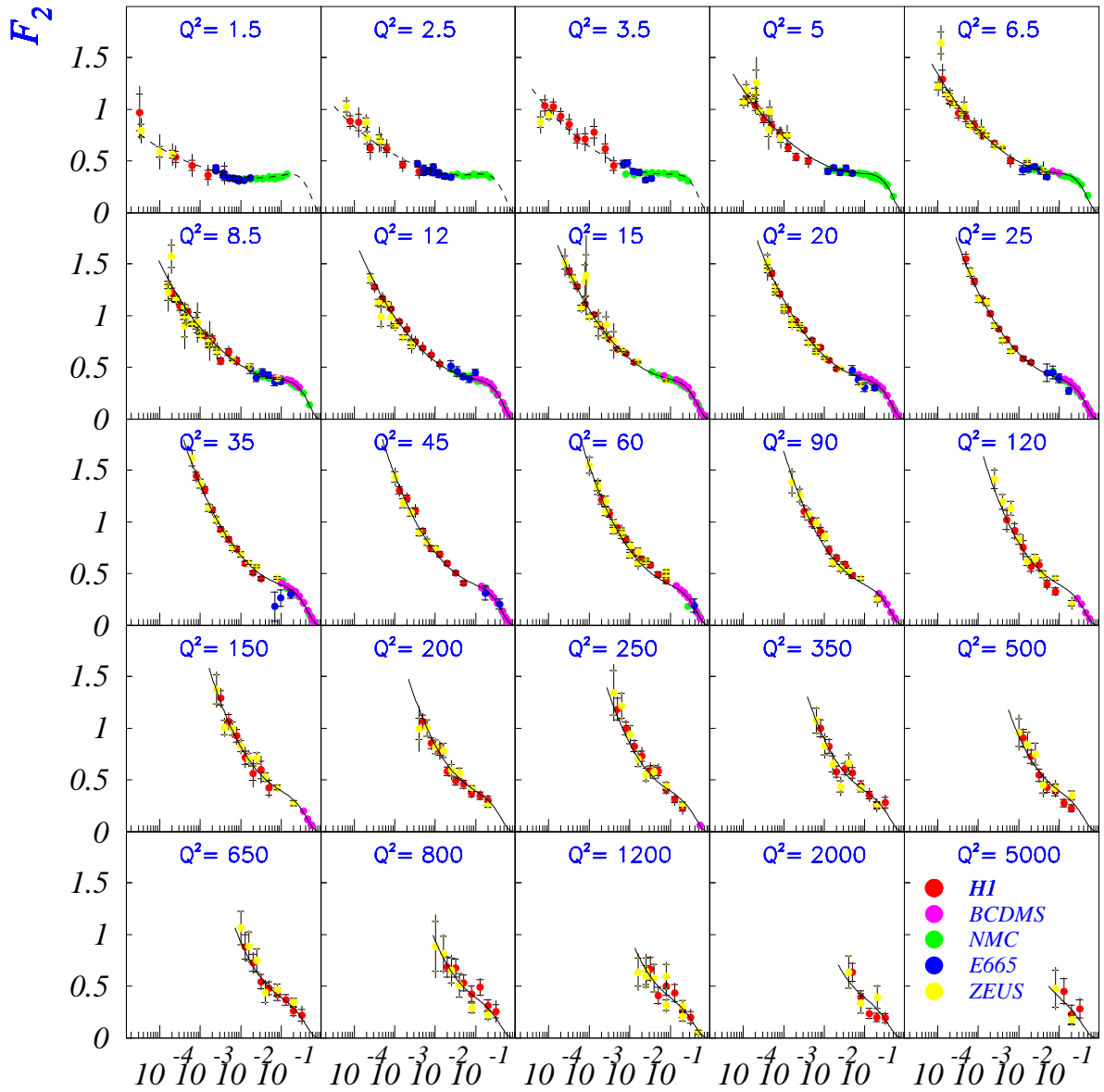


Figure 4: Measurement of $F_2(x, Q^2)$ as function of x .

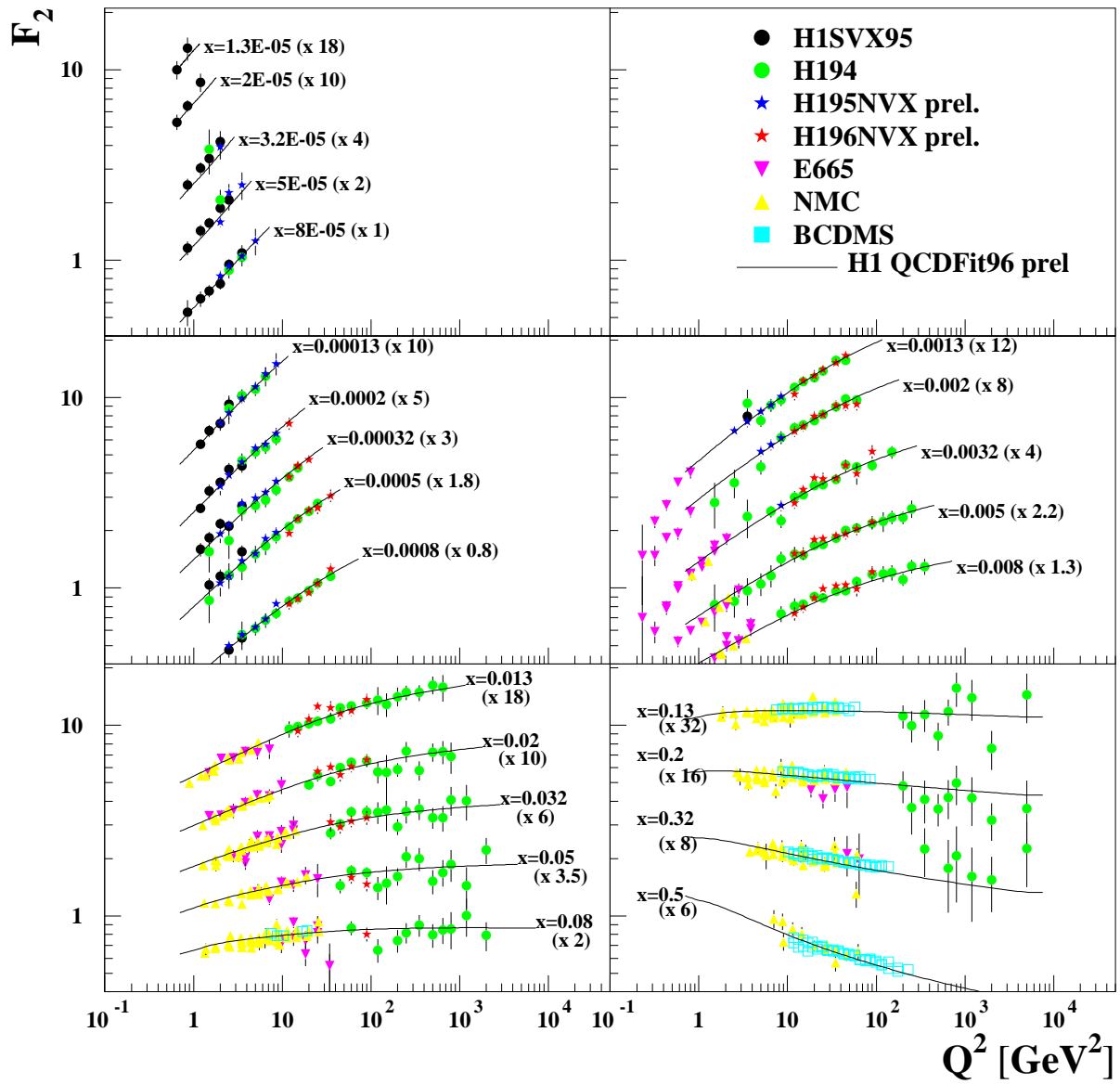


Figure 5: Measurement of $F_2(x, Q^2)$ as function of Q^2 .

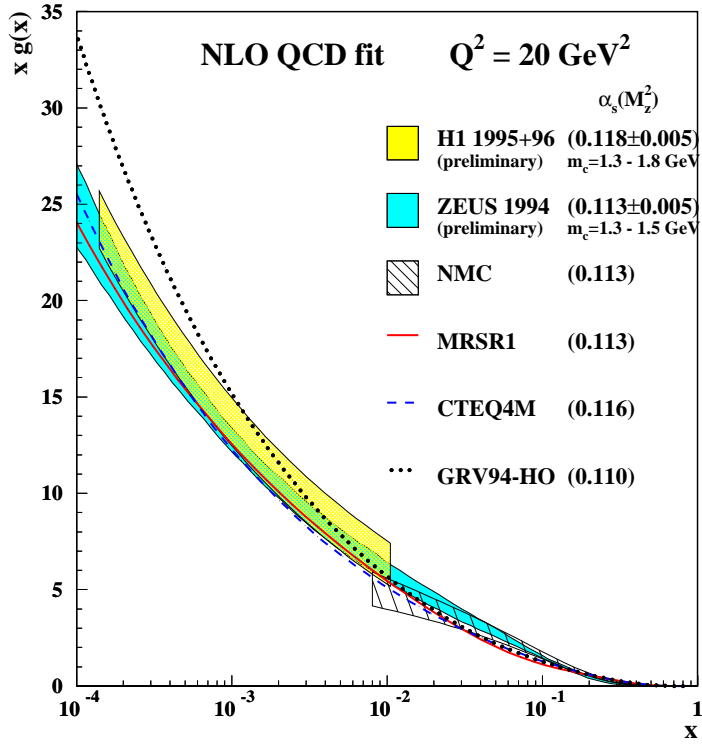
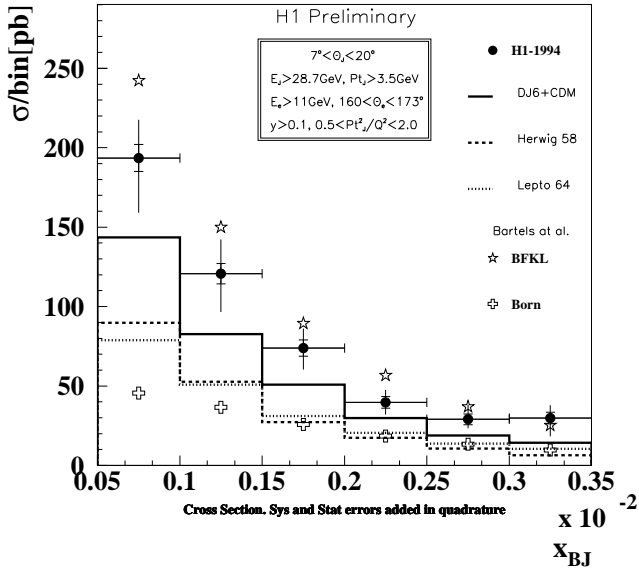
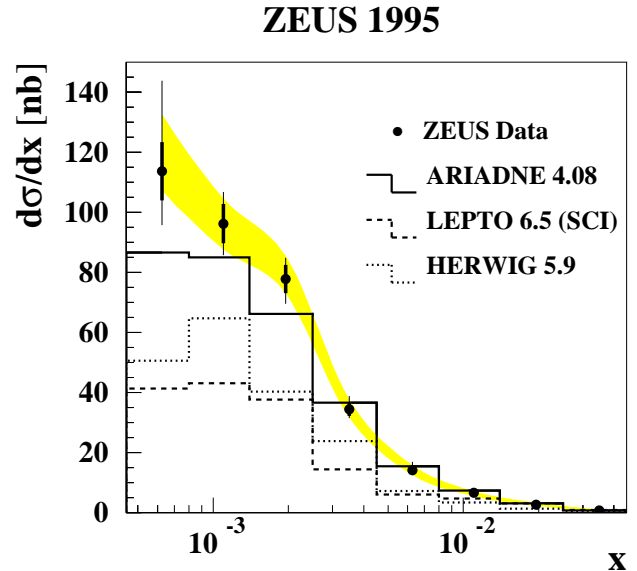


Figure 6: The gluon density $xg(x)$ at $Q^2 = 20 \text{ GeV}^2$ extracted from NLO QCD fits by the H1, ZEUS and NMC collaborations.



(a)



(b)

Figure 7: Measurement of forward jet production as function of x by (a) H1 and (b) ZEUS experiments. The errors due to the uncertainty in the jet energy scale are show in the shaded band.

ZEUS 1994-97 Preliminary

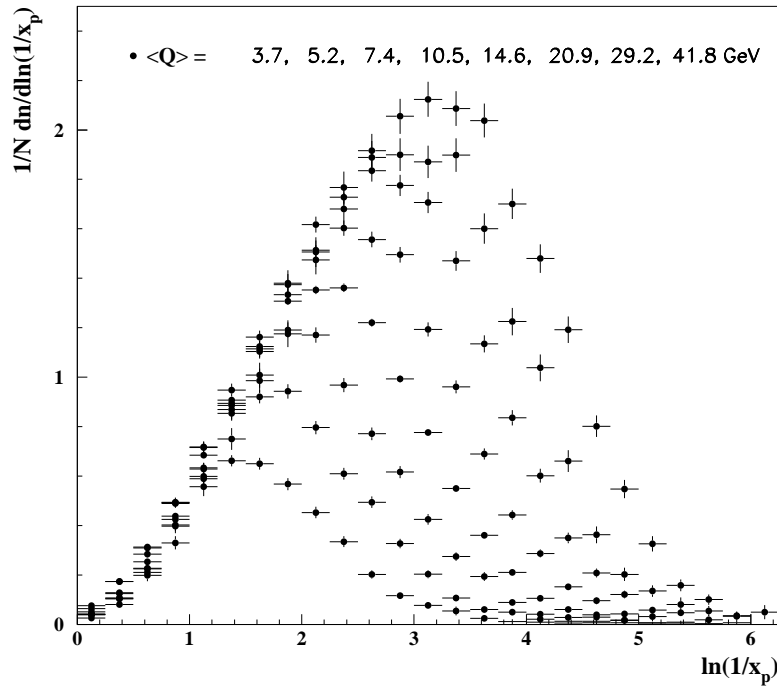


Figure 8: Preliminary ZEUS results of the evolution of the $1/N dn/d\log(1/x_p)$ distributions with Q^2 . Only statistical errors are shown.

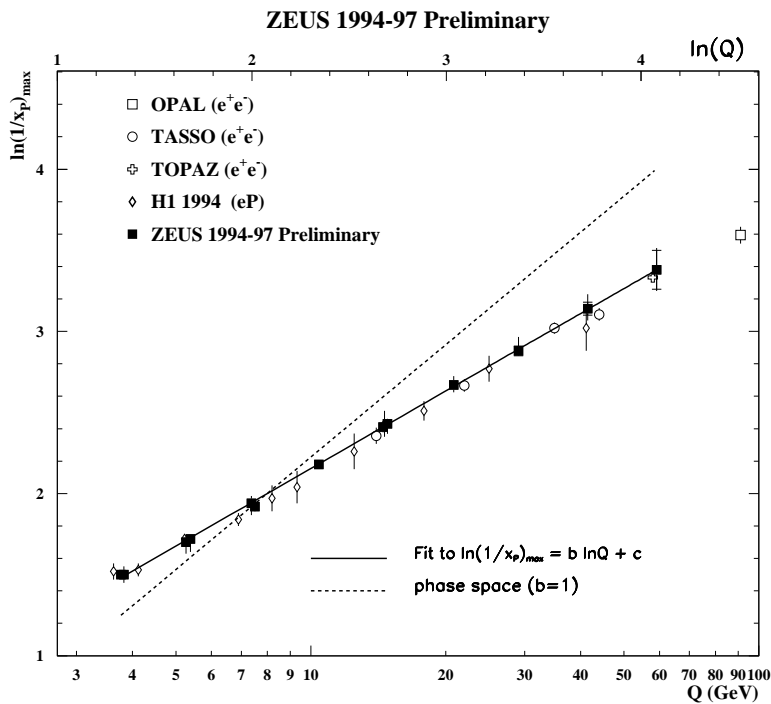


Figure 9: Preliminary ZEUS results of evolution of the peak position $\log(1/x_p)_{max}$ with Q^2 .

ZEUS 1994-97 Preliminary

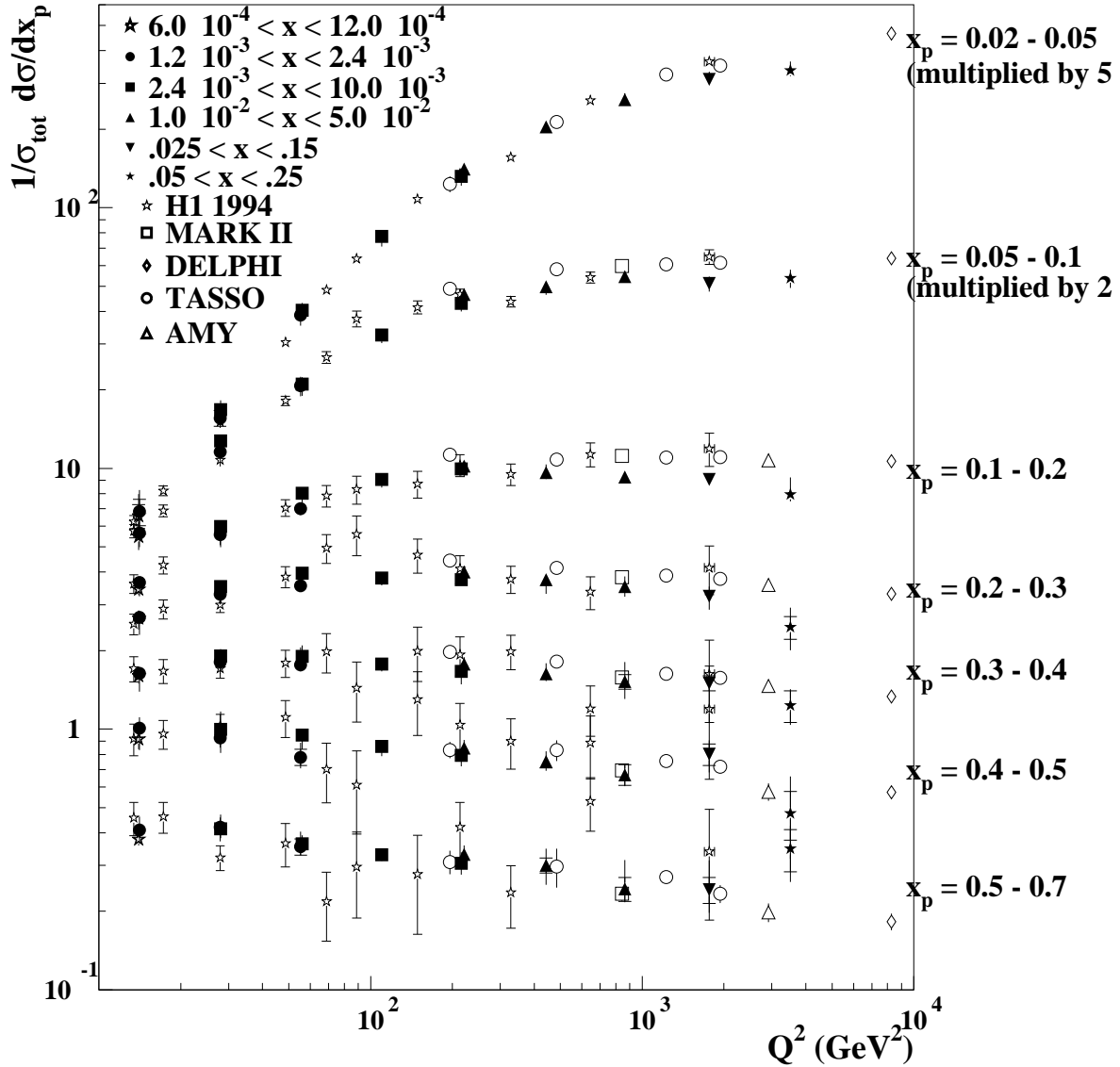


Figure 10: The inclusive charged particle distribution, $1/\sigma_{tot} d\sigma/dx_p$, in the current fragmentation region of the Breit frame as measured by H1 and ZEUS collaborations. The open points represent data from e^+e^- experiments divided by two to account for q and \bar{q} production (also corrected for contributions from K_S^0 and Λ .)